Electronic structure, photoemission, inverse photoemission, and x-ray emission spectra of superconducting $Ba_{1-x}K_xBiO_3$

Noriaki Hamada,* Sandro Massidda, and Arthur J. Freeman
Department of Physics and Astronomy and Materials Research Center, Northwestern University, Evanston, Illinois 60208

Joseph Redinger
Institute für Technische Elektrochemie, Technische Universität Wien, 1060 Wien, Austria
(Received 1 May 1989)

The electronic structure of $BaBiO_3$ is calculated by using the full-potential linearized augmented-plane-wave method in the local-density approximation, and the alloying effect of K additions is considered using the simple rigid-band model. The electron-phonon mechanism for the superconductivity is discussed within the rigid muffin-tin approximation. In this context, the difference of the electronic structure from the cuprate high-T_c materials is elucidated in detail. Photoemission, inverse photoemission, and x-ray emission spectra are compared with experiment to check the validity of the single-particle picture for these excitations.

I. INTRODUCTION

The discovery of the high-T_c (30 K) copperless superconductor,[1,2] $Ba_{1-x}K_xBiO_3$, has introduced new aspects into the discussion of the mechanism of high-T_c superconductivity. In this noncuprate material, the Bi atoms, which are octahedrally coordinated to oxygen, are expected to play the role of the Cu atom in the Cu-O high-T_c materials.[3-5] Instead of the $3d$ states of Cu, the $6s$ states of Bi are strongly mixed with $2p$ states of O, as will be discussed later. Therefore, both magnetism and strong electron correlation (which are both missing) are not expected to be essential for the superconductivity.

Recent observations[6,7] of an isotope effect on T_c by ^{18}O substitution in $Ba_{1-x}K_xBiO_3$ have added a new point of interest into understanding superconductivity in this material. However, the two existing experimental reports do not agree on the value of the α exponent ($T_c \sim M^{-\alpha}$), giving $\alpha \sim 0.2$ (Ref. 6) and $\alpha \sim 0.4$,[7] respectively. Since the existence of an isotope effect clearly relates superconductivity to the lattice vibrations, a definite experimental answer is clearly of great interest. It is, in fact, crucial to determine whether the superconductivity of $Ba_{1-x}K_xBiO_3$ is due to the electron-phonon mechanism only (in which case the theoretical limit would have been reached) or if another mechanism (possibly common to high-T_c Cu-O materials) is at work.

It is now accepted that the superconducting state of these materials must be understood on the basis of details of their crystallographic structure. In this sense, band-structure calculations for the normal state provide important information which can help the understanding of the superconducting state. In what follows, we will find similarities and differences of the electronic structure of these materials which are closely related to their superconducting state.

The crystal structure of $Ba_{1-x}K_xBiO_3$ is cubic perovskite,[2,8-10] which implies that low dimensionality is not necessary for T_c values around 30 K. Together with the parent system $BaPb_{1-y}Bi_yO_3$ ($y \sim 0.25$),[11,12] $La_{2-x}Ba_xCuO_4$,[3] and the cubic spinel $Li_{1+z}Ti_{2-z}O_4$,[13] $Ba_{1-x}K_xBiO_3$ ($x \sim 0.3$) has a structural similarity consisting of a (sometimes distorted) octahedral coordination of the metal atom to six O atoms. The other cuprate high-T_c materials have similar structures with pyramids consisting of five O atoms around a Cu atom or sometimes completely miss the apical oxygens and have planar square coordination.

The band structure for $Ba_{1-x}K_xBiO_3$ has already been calculated by Mattheiss and Hamann,[14] who showed using several supercells that the effect of the K alloying is well described within a rigid-band model. In this paper, we present results of highly precise local-density calculations for $BaBiO_3$, describe K alloying by means of the rigid-band model, and present measurable quantities which can be compared in detail with experiment, especially photoemission, inverse photoemission, and x-ray emission spectra. On the basis of our calculated precise single-particle quantities, we will discuss the superconductivity by considering the electron-phonon and other mechanisms.

In Sec. II, we present results of the band-structure calculations by the full-potential linearized augmented-plane-wave (FLAPW) method[15] in the local-density approximation (LDA). The result of single-step x-ray photoemission calculations are compared with experiment in Sec. III. Section IV is devoted to discussing the superconductivity in the K-doped materials and other properties which may be compared with experiment.

II. BAND STRUCTURE OF $Ba_{1-x}K_xBiO_3$

The electronic structure of $BaBiO_3$ was calculated for the cubic perovskite structure using the highly precise full-potential linearized augmented-plane-wave method[15]

with the Hedin-Lundqvist exchange-correlation potential. The lattice constant is assumed to be 4.2932 Å, which corresponds to the lattice parameter of $Ba_{1-x}K_xBiO_3$ with $x=0.29$. [This x value was shown by neutron-diffraction structural analysis[8] to be the final composition corresponding to the maximum T_c value (initial K composition $x=0.4$).] The Ba atom is situated at the corner of the cube, Bi is at the body center, and the O atoms are at the face centers. Inside the muffin-tin spheres, the angular-momentum expansion was truncated at $l=8$ for the wave functions and $l=6$ for the charge density and potential. In the interstitial regions, about 3400 reciprocal-lattice vectors are considered in the Fourier representation of the charge density and potential. The LAPW functions with the wave vectors $|\mathbf{k}+\mathbf{G}| \leq K_{\max}=3.6$ a.u. are used in the expansion of the eigenfunctions leading to about 420 basis functions. Fifty inequivalent sampling k points and the linear tetrahedron scheme are used for the Brillouin-zone integration during the self-consistent iterations. The density of states is calculated using 80 k points in the irreducible wedge of the Brillouin zone.

A. Energy bands

Figure 1 shows the band structure. As in the cuprate superconductors, just one antibonding band crosses the Fermi energy (E_F); it has a wide dispersion due to the strong hybridization between the Bi 6s and O 2p states. This hybridization is, in fact, symmetry forbidden at Γ, where the (Γ_1) Bi 6s states cannot interact with the (Γ_{15}, Γ_{25}) neighboring O 2p states. However, in going along the Γ-X-M-R directions, such an interaction is progressively more allowed. In this respect, the Bi-O $sp\,\sigma$ band here is similar to the Cu-O $dp\,\sigma$ antibonding band crossing E_F in the Cu oxide superconductors; also in that case, in fact, copper and oxygen states were nonbonding at Γ and strongly antibonding at the (in-plane) zone boundaries. The dimensionality factor, however, makes the difference between the two cases. The charge density for this band averaged over the Fermi surface corresponding to $x=0.29$ is shown in Fig. 2. No charge density is found at the Ba site; the conduction occurs through a three-dimensional network consisting of Bi 6s and O 2p states. This feature does not change for small changes in the Fermi level.

The bonding counterpart of Bi 6s and O 2p is situated from -7 to -13 eV below the Fermi energy. The nonbonding or weakly bonding O 2p states are located around -2.5 eV. The bandwidth due to the direct hybridization of these O 2p states is small (~ 2 eV) compared with the case of cuprate high-T_c materials in which the weakly bonded O 2p bandwidth is as large as 6 eV. Along the Γ-X-M-Γ lines, there is a very flat band at -7 eV, which is due to the $pp\sigma$ bonding combinations of the Bi 6p and O 2p orbitals; this band rises up in energy along the Γ-R direction because the bonding contribution of the Bi 6p state disappears at the R point by symmetry. The states at -12 eV are due to the Ba 5p semicore electrons. Bands higher than 2 eV above E_F consist of Ba 5d

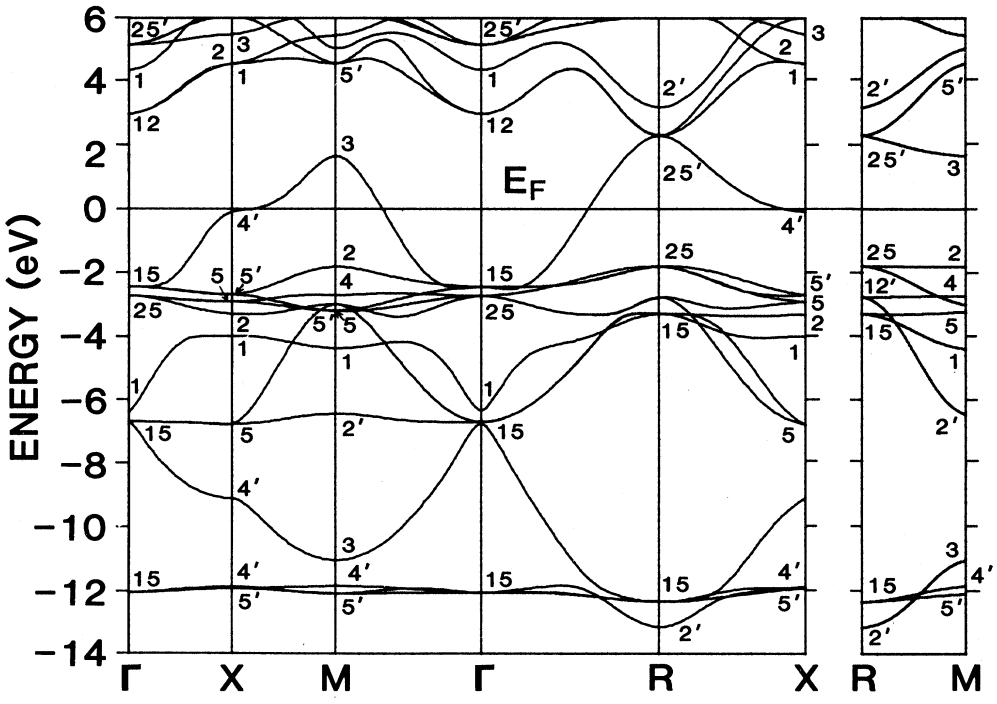

FIG. 1. Electronic band structure of $BaBiO_3$ along the main symmetry lines of the Brillouin zone and corresponding to the lattice constant of $a=4.2932$ Å. The symmetry labels correspond to choosing the origin at the Ba site.

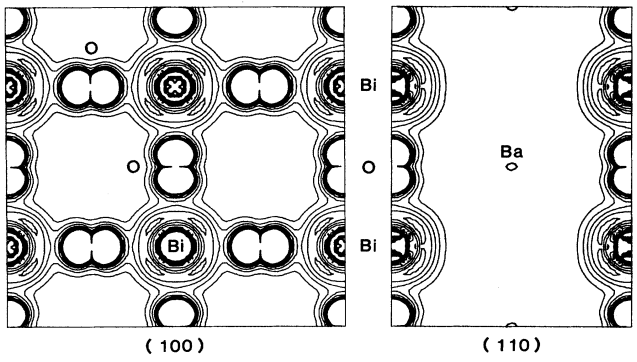

FIG. 2. Average charge density of the states at the Fermi energy of $Ba_{1-x}K_xBiO_3$ for $x=0.29$.

and Bi 6*p* states. The whole band structure is very similar to the results of Mattheiss and Hamann.[14]

The states of the Ba site do not contribute to the band near the Fermi energy. Furthermore, Mattheiss and Hamann showed, using supercell calculations,[14] that the K 3*p* state appears at the same energy as the Ba 5*p* state. Therefore, a rigid-band model is a good approximation over the whole valence band for the $Ba_{1-x}K_xBiO_3$ system and will be used in the following discussion.

B. Density of states

Figure 3 shows the total density of states (DOS) and some of the partial DOS (PDOS) for Bi and O. The sharp peak of the total DOS at -12 eV is due to the Ba 5*p* corelike states. The broad peak from -13 to -7 eV comes from the bonding states of the Bi 6*s* and O 2*p* orbitals, as is shown in the PDOS in the figure. The O 2*p* and Bi 6*p* bonding states produce the peak around -6 eV. The large peak from -4 to -2 eV comes from the nonbonding states of O 2*p*; its width is mainly due to the direct mixing between the O 2*p* states. There is a small contribution of Ba 6*s* to the peak at -4 eV. The broad peak from -2 to 2 eV consists of the antibonding Bi 6*s* and O 2*p* states. The states above 2 eV consist of Ba 5*d* and Bi 6*p*. In this region, we can see a trace of the mixing between Bi 6*p* and O 2*p* in the partial DOS.

Figure 4 shows in expanded detail the total DOS around the Fermi energy. A peak just below E_F at $x=0$ corresponds to the three-dimensional saddle-point singularity (SPS) at the X point. The Fermi energy for $x=0.29$ is situated well below this peak. The coincidence of E_F with such a peak provides an explanation for the structural phase transition of cubic $BaBiO_3$ to its observed stable monoclinic, semiconducting structure. In fact, Mattheiss and Hamann[16] showed that this structural change including the frozen phonon breathing mode of O octahedra can open up a gap; the calculated gap is actually almost zero, possibly because of limitations of the local-density approximation and the uncertainty of the numerical calculations. The density of states at E_F, $N(E_F)$, for $x=0$ and $x=0.29$ are 0.828 and 0.555 states/eV cell, which is (per Bi atom) smaller than those

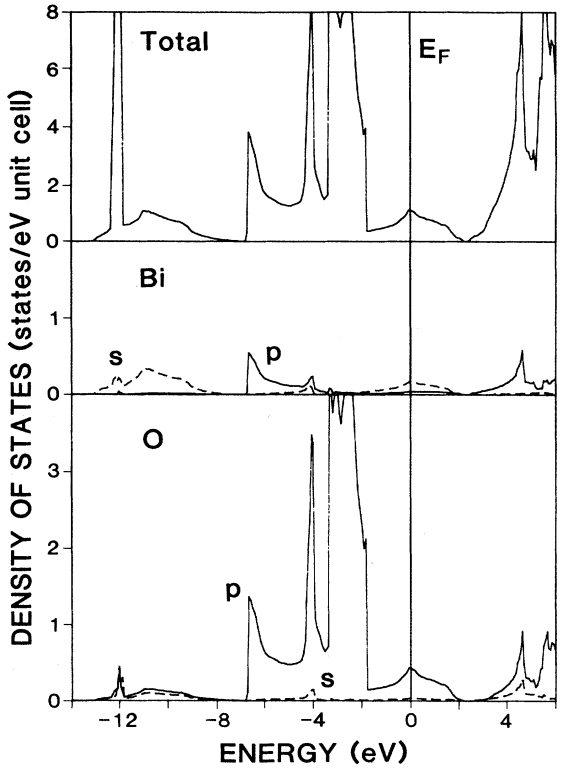

FIG. 3. Total and partial densities of states for $Ba_{1-x}K_xBiO_3$. The Fermi energy corresponds to $x=0$.

[~1 states/eV per Cu atom (Refs. 17–22)] of the cuprate high-T_c oxides, but larger than that of the $BaPb_{1-y}Bi_yO_3$ system with y around 0.25. The muffin-tin projected contributions to the density of states at E_F, summarized in Table I, provide clear evidence for the O *p*–Bi *s* hybridization. The Bi contribution is smaller than the O contribution for $(BaK)BiO_3$, while the Cu contribution is larger than the O contribution for the cuprate materials. This is

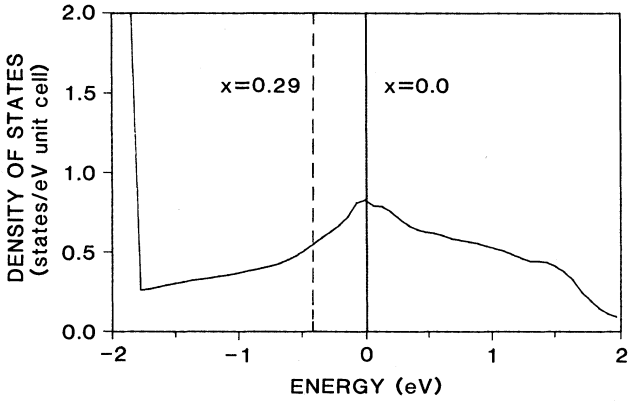

FIG. 4. Total density of states of $Ba_{1-x}K_xBiO_3$ using a rigid-band model close of E_F. The Fermi energies are shown for both $x=0$ and $x=0.29$.

TABLE I. l-decomposed atomic contribution inside muffin-tin spheres ($R_{Bi}=2.45$ a.u., $R_0=1.60$ a.u.) to the DOS at E_F in states/eV cell.

	$x=0$			$x=0.29$		
	s	p	d	s	p	d
(Ba,K)	0.000	0.000	0.000	0.000	0.000	0.000
Bi	0.176	0.044	0.020	0.115	0.033	0.011
O	0.033	0.432	0.004	0.024	0.285	0.003
Total DOS		0.828			0.555	

because the atomic Bi 6s level is located deep in energy relative to the O 2p level, while the atomic Cu 3d level is very close to the O 2p level. However, the metal-oxygen hybridization here is much stronger than[23] in $Li_{1+x}Ti_{2-x}O_4$.

C. Fermi surface

The Fermi surfaces (FS) of stoichiometric $BaBiO_3$ and of $Ba_{0.71}K_{0.29}BiO_3$ (calculated using a rigid-band model) are shown in Fig. 5(a) and 5(b), respectively. The presence of K lowers E_F and correspondingly induces the change of the FS topology seen in Fig. 5(b) when E_F crosses the three-dimensional saddle-point singularity at the point X in the Brillouin zone for $x\sim 0.1$.

Some FS nesting can be observed, due to the flat portion of the FS perpendicular to the Γ-M direction. The corresponding spanning vector is not commensurate. The perfect FS nesting found in the two-parameter tight-binding model of Mattheiss and Hamann[16] for cubic $BaBiO_3$ is not found in the present FLAPW results. At $x=0.29$, corresponding to the reported maximum value[8] of T_c and away from the SPS structural instability, the FS is rather free-electron-like (i.e., a somewhat flattened sphere).

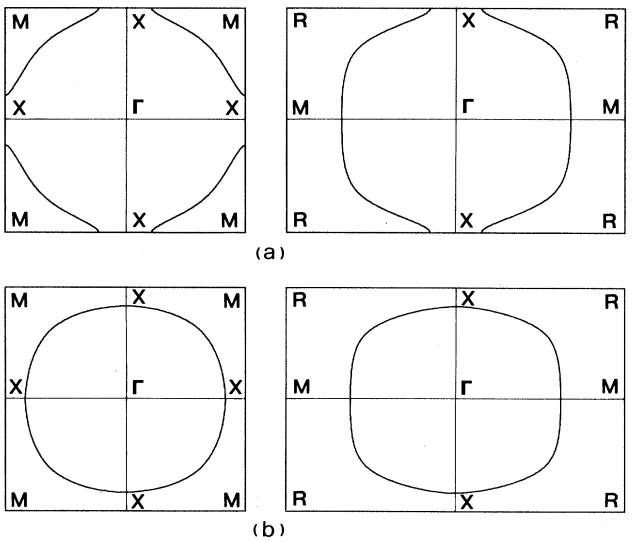

FIG. 5. Fermi surfaces of $Ba_{1-x}K_xBiO_3$ for (a) $x=0$ and (b) $x=0.29$.

III. CALCULATED PHOTOEMISSION, INVERSE PHOTOEMISSION, AND X-RAY EMISSION SPECTRA

In this section we present calculated photoemission (PES), inverse photoemission (IPES), and x-ray emission (XES) spectra for $Ba_{1-x}K_xBiO_3$ which may be directly compared with their experimental determinations. The single scatterer final-state approach (SSFSA) underlies our calculation of PES and IPES; von Barth's final-state rule was assumed to be valid for XES. Since both approaches have been discussed extensively in the literature,[24–32] only the basic features are recalled here. The same single-particle LDA Hamiltonian is used to describe the hole and electron dynamics of the initial and final states. This means that all the well-known problems of identifying LDA eigenvalues with real quasiparticle excitations still persist in the calculated spectra. In the SSFSA, the outgoing photoelectron only feels the potential at the site of its creation but further scattering on its way through the crystal is discarded. Performing an angular integration and assuming, furthermore, that the transition matrix elements are independent of the direction of the outgoing photoelectron, the photocurrent may be written as a sum of SSFSA matrix element weighted partial density of states (DOS). It should be noted, however, that since the isotropic SFFSA matrix elements may differ by orders of magnitude for the individual constituents, scattering channels, and photon energies, often a particular l component of the total DOS is strongly enhanced. The SSFSA is certainly best suited for high photon energies in the x-ray photoemission (XPS) regime and angle-integrated measurements performed on polycrystalline samples. For the lower photon energies [typically in the ultraviolet photoelectron spectroscopy (UPS) regime], both of the above assumptions inherent in the SSFSA are less justified; still we believe that performing an angle-integrated measurement on a polycrystalline sample brings about enough averaging to make the SSFSA a meaningful first step.

In the case of XES, the final-state rule simply states that the initial core hole does not affect the resulting spectrum and rather the local l-dependent final-state DOS is seen in the spectra. The final-state DOS may be identified with the LDA ground-state DOS provided the valence-band hole is well screened.

Previous experience with both approaches shows that they work surprisingly well for p-d bonded systems like

the $3d$ and $4d$ transition-metal carbides and nitrides,[24,32] and some transition-metal compounds and alloys. In all these materials the d electrons may be considered as itinerant. Until recently, both approaches did not seem to do so well in treating the Cu(d)–O(p) bonded high-T_c superconductors;[28–31] rather large discrepancies were found to show up in the Cu(d) dominated spectra, such as XPS. This was understood on the basis of evidence that the Cu d band is not completely filled, but contains a hole, which interacts with the photo hole generated in the photoemission process. This final-state effect not only causes valence- and core-level satellites, but also the unusually large differences between theory and experiment regarding the valence-band binding energies. However, the latest results on single crystals cast some doubts on the magnitude of this large valence-band binding-energy difference, since part of the discrepancy may be traced back to charging effects due to an insulating surface.[33–34] Yet, there is no doubt that hole-hole interaction is important in a not completely filled Cu-d band, as clearly demonstrated by comparing PES, IPES, and Auger spectra for Cu(d^9)O and Cu(d^{10})$_2$O.[35] Anyway, and of importance for this study, correlation effects in an unfilled d band are not operative in the $Ba_{1-x}K_xBiO_3$ superconductor.

All the calculations have been performed nonrelativistically although relativistic core wave functions have been used in the calculation of the XES spectra. All the wave functions needed for matrix elements were computed employing FLAPW potentials subjected to the self-consistent muffin-tin methods. The finite lifetime of the valence and core holes were taken into account by convoluting the spectra by an energy-dependent Lorentzian with full width at half-maximum (FWHM) taken as $\Gamma(E)=\Gamma_c+\Gamma_v(E)$; here c and v denote the core and valence holes, respectively. $\Gamma_v(E)$ increases linearly as[36] $0.2(E_F-E)$ eV and $\Gamma_c\neq 0$ only for XES. No lifetime broadening was taken into account for IPES. Finally, a Gaussian spectrometer resolution was taken into account with FWHM representative for the actual experiment.

A. Photoemission spectra

We show in Fig. 6 the Al $K\alpha$ ($h\nu=1487$ eV) XPS spectrum for $Ba_{1-x}K_xBiO_3$ as calculated within the SSFSA. Photoemission spectra have been recorded[37] for the related $BaPb_{1-y}Bi_yO_3$ system including pure $BaBiO_3$. In a rigid-band treatment, E_F is shifted upwards by 0.43 eV for $Ba_{1-x}K_xBiO_3$ upon decreasing x from 0.29 to zero. The calculated changes in the spectrum are indicated by the dotted line. Basically, two prominent features dominate the spectrum.

(i) Emission from the valence bands gives rise to a broad structure with a maximum around -3 eV (with respect to E_F for $BaBiO_3$) and shows a shoulder around -6 eV and another faint shoulder at -4 eV. The intensity is lowest around -7.5 eV and rises again for larger binding energies.

(ii) Emission from the spin-orbit split Ba $5p_{3/2}$, Ba $5p_{5/2}$ doublet is centered at -12.3 eV.

At this point, a remark on the calculation of the Ba $5p$ emission is in order. In the FLAPW calculation, the Ba $5p$ states were treated semirelativistically as band states neglecting spin-orbit splitting. In order to facilitate comparison with experiment, especially with respect to the relative intensities between the Ba $5p$ emission and emission from the valence band, we added spin-orbit splitting *a posteriori*. As the Ba $5p$ band is rather narrow, a simple atomiclike procedure was chosen. The semirelativistic FLAPW Ba $5p$ partial DOS was spin-orbit split by 1.99 eV as determined by an atomic calculation for the FLAPW potential [the experimental value is 1.9 eV (Ref. 37)] and keeping the center of gravity fixed at the maximum of the original semirelativistic Ba $5p$ DOS. The occupation of the Ba $5p_{1/2}$ and Ba $5p_{3/2}$ DOS was taken to be 2 and 4 electrons, respectively. The lifetime of the Ba $5p$ hole was fixed at 0.2 eV.

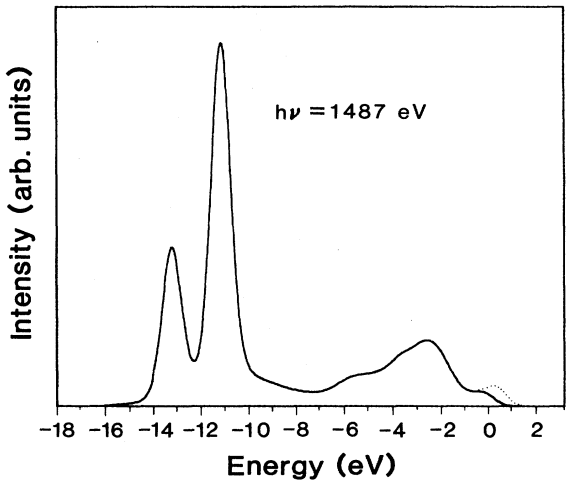

FIG. 6. Calculated valence-band XPS spectrum for $Ba_{1-x}K_xBiO_3$; solid line $x=0.29$, dotted line $x=0$.

Upon comparing now the calculated spectrum with the experimental XPS spectrum of Ref. 37, we recognize that the overall agreement is very good indeed. Still, there are two features in the calculated spectra which deviate from experiment. The shoulder close to the onset of the Ba $5p$ emission due to the bonding Bi(s)–O(p) states around -10 eV is not matched by the calculation. This discrepancy has a trivial origin, however, and may be easily traced back to the well-known inherent problems of identifying LDA eigenvalues with quasiparticle excitations by neglecting the self-interaction corrections (SIC) for rather tightly bound electrons. In the calculation, the Ba $5p$ emission is placed at too low a binding energy (by 1.65 eV) and yields an appreciable intensity already at -10 eV, thereby filling the plateau seen in the experimental spectrum. Since the Ba $5p$ states are almost atomiclike, we tried to find an estimate for the SIC by comparing total-energy differences with the atomic LDA eigenvalues. For a neutral Ba atom the correction amounts to -3.4 eV and increases for a "bare" Ba^{2+} ion to -4.4 eV. Both values are too high and demonstrate that the Ba $5p$ holes in $BaBiO_3$ are very effectively screened by the surrounding highly polarizable oxygen ions.

The other discrepancy concerns the region around E_F. The calculated intensity is rather high as compared with the experimental findings.[37] This is consistent, however, with the fact that $BaBiO_3$ is calculated to be metallic instead of semiconducting. The origin of the semiconducting gap was attributed to frozen-in breathing-mode distortions of the oxygen octahedra,[16] as well as to spin-density wave formation at the Bi site for the Bi-rich alloys.[38] The latter mechanism implies a rather large correlation energy for the Bi 6*s* electrons, so that screening of the long-range Coulomb interaction by the doped itinerant carriers is not so effective[39] and might lead to a suppression of the DOS near E_F also for the metallic K-doped $BaBiO_3$.

Consider now Fig. 7 which exemplifies the photon-energy dependence of the valence-band PES. For that reason the atomiclike Ba 5*p* states have been excluded. The XPS spectrum shown in the top panel is made up from a large Bi contribution overlaid by O 2*p* and Ba 6*p* emission around -3 eV. The Bi emission is *s*-like at -10 eV and at E_F. The Bi maximum at -3 eV is largely due to *d* states and the -6 eV shoulder the Bi 6*p* states. It may be worth noting that the oxygen component of the -10-eV peak and also close to E_F is mainly *s*-like because the O-*s* matrix element is about ten times larger than the O-*p* matrix element. As the photon energy is lowered to 70 eV (middle panel), emission from the O 2*p* states becomes the dominant contribution, which results in an apparent narrowing of the spectrum. The largest difference between the 70-eV spectrum and the 21.1-eV spectrum (bottom panel) is caused by the different spectrometer resolution used (0.8 eV for 70-eV and 1487 and 0.4 eV for 21.2-eV photon energy). The narrowing caused by the diminished Bi contribution is also found in experimental spectra on the related $BaPb_{1-y}Bi_yO_3$ system.[40]

B. Inverse photoemission spectra

Consider now the inverse photoemission results for the unoccupied bands as shown in Fig. 8. The photon energies used in the calculation represent two typical energies accessible in experiment. The SSFSA should again be rather accurate for the high photon energy of 1487 eV, but obviously a photon energy of 9.7 eV pushes the validity of the SSFSA to its limits. However, we are still convinced that taking the spectra from polycrystalline samples will bring about the necessary averaging and thus render the SSFSA not too bad an approach even for the extremely low photon energy of 9.7 eV.

At a first inspection, we see that both spectra look very similar despite the large difference of photon energies. The dissimilarities are brought about mainly by the different experimental resolutions assumed (0.8-eV FWHM at 1487 eV and 0.4 eV at 9.7 eV are fair estimates

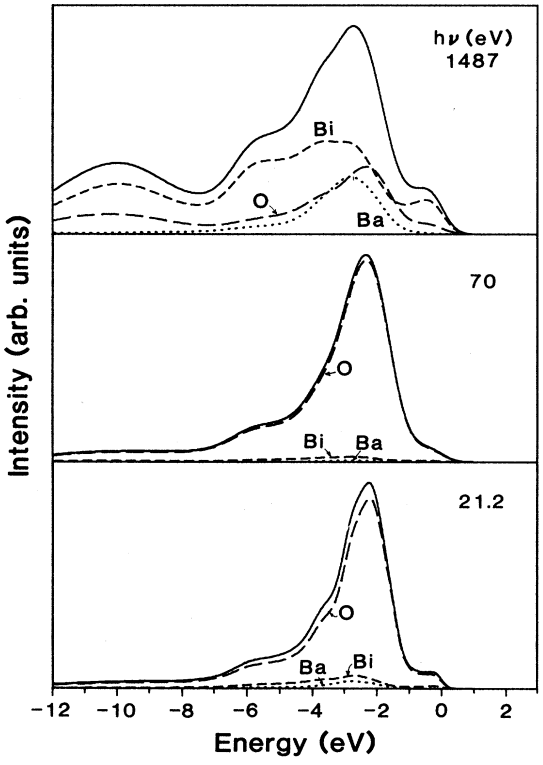

FIG. 7. Calculated valence-band PES spectra for $Ba_{1-x}K_xBiO_3$ ($x=0.29$). The atomiclike Ba 5*p* states have been omitted. The solid line corresponds to the total spectrum and the dashed and the dotted lines indicate the major contributions as shown in the figure.

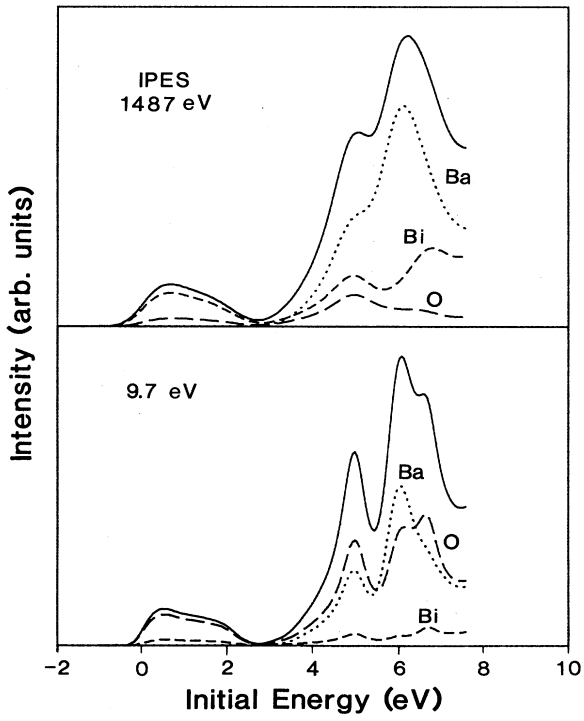

FIG. 8. Calculated inverse PES spectra for $Ba_{1-x}K_xBiO_3$ ($x=0.29$). The solid lines corresponds to the total spectrum and the dashed and dotted lines indicate the dominant contributions as shown in the figure.

of typical experimental resolutions obtained by present day spectrometers). We distinguish two peaks around 1 and 6 eV above E_F. The peak at lower energy is due to the unoccupied part of the Bi $6s-O\,2p$ antibonding band separated by a deep minimum at 2 eV from the upper peak composed of O, Bi, and Ba admixtures. Although the overall shape of the two spectra is very similar, the partial contributions are quite different due to the different weighting by the SSFSA matrix elements. For the 1-eV peak the relative importance of the Bi and O emission is reversed by the matrix elements. For 9.7-eV photons, the O $2p$ states give the strongest contribution with a little Bi $6s$ admixture, whereas for 1487-eV photons O $2p$ emission is completely negligible and the oxygen contribution arises from the O s channel. As a consequence, the oxygen contribution to the higher 6-eV peak is also quite different for 9.7- and 1487-eV photons, reflecting the O $2p$ and O s DOS, respectively. The loss of intensity due to the lower O contribution for the 6-eV peak is compensated by an increased Bi contribution which arises mostly from Bi $2p$ states. The Ba contribution shows no preference for one channel or the other and its intensity is distributed among the s,p,d channels, but we may say that Ba $5d$ becomes more important for lower photon energies.

With regards to possible agreement with experiment, we may only speculate since there are no experimental data available so far. We are aware of three possible sources of "disagreement."

(i) An incorrect description by the LDA of the antiscreening of the added extra electron for states above E_F. The calculation places the peaks too close to E_F.

(ii) The presence of K $3d$ states (which remain unaccounted for in the rigid-band treatment) may very well contribute to the spectra at higher energies. For ordered tetragonal $Ba_{0.5}K_{0.5}BiO_3$, no unoccupied K states are found below 4 eV.[14]

(iii) In contrast to PES, many-body effects such as hole-hole repulsion in the final state are not expected to play a very important role, since holes are filled by the impinging electrons. This should be particularly true for the 1-eV peak. It may be interesting to note in this context that even for CuO (Ref. 35) (which might be thought of as the parent compound to all the Cu-based high-T_c superconductors), single-particle band theory fared well in describing the experimental IPES. The same was true for $YBa_2Cu_3O_7$.[29]

C. X-ray emission spectra

Since a localized core hole is involved in the emission process, no k-dependent information is carried by the emitted photons and only the selection rules for the dipole transition from the valence band to the core hole apply. Therefore x-ray emission spectra provide a direct access to the local l-dependent partial DOS and hence are easier to interpret than are photoemission spectra. By selecting the proper core levels all the important components of the total DOS may be mapped out. The only severe drawback in using this method is posed by the finite lifetime of the core hole, which must be sufficiently long lived so as not to introduce too much additional broadening. For this reason, Bi $4p$ or $5p$ states cannot be used to detect the Bi $6s$ DOS. We have chosen the O $1s$ [$\Gamma_c=0.15$ eV (Ref. 41)], Ba $3d_{5/2}$ ($\Gamma_c=0.45$ eV), Ba $4d_{(3/2,5/2)}$ [$\Gamma_c=0.2$ eV (Ref. 37)], Bi $4f_{(5/2,7/2)}$ [$\Gamma_c=0.2$ eV (Ref. 37)], and the Bi $5d_{(3/2,5/2)}$ ($\Gamma_c=0.2$ eV) core holes giving rise to the O-K, Ba-M_5, Ba-$N_{4,5}$, Bi-$N_{6,7}$, and Bi-$O_{4,5}$ spectra, respectively. The resulting spectra have been convoluted by a Lorentzian with FWHM of $\Gamma_c+\Gamma_v(E)$ accounting for core (Γ_c) and valence hole (Γ_v) lifetimes. $\Gamma_v(E)$ was taken to be the same as in the case of the PES spectra. Finally, a Gaussian spectrometer resolution of FWHM equal to 1 eV was employed.

The calculated O and Ba related XES spectra for $Ba_{1-x}K_xBiO_3$ ($x=0.29$) are shown in Fig. 9. As the O K spectrum mirrors only the O $2p$ DOS its similarity to the 70-eV PES spectrum is obvious. The Ba M_5 spectrum maps transitions into a Ba $3d_{5/2}$ core hole predominantly from the small Ba p valence-band DOS. Since the FLAPW calculation was done semirelativistically (no spin-orbit splitting was considered in the valence band), nonrelativistic dipole selection rules were applied. The matrix elements, however, have been calculated using relativistic core wave functions. The Ba $N_{4,5}$ spectrum con-

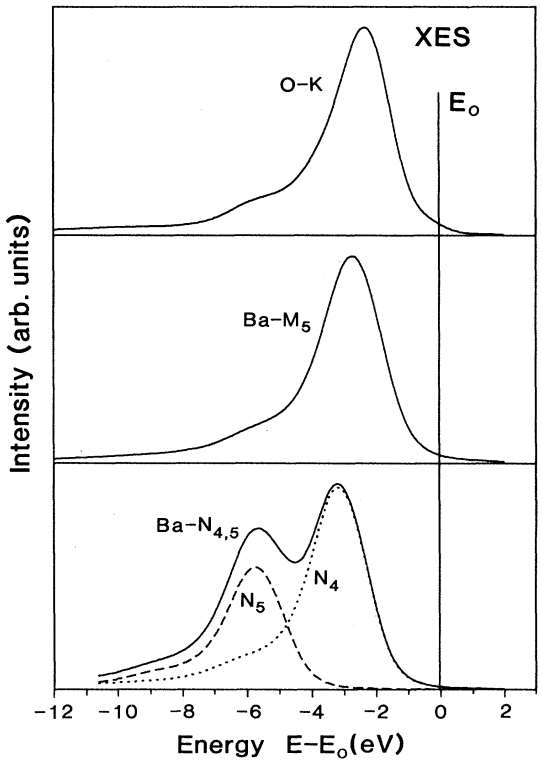

FIG. 9. Calculated x-ray emission spectra for $Ba_{1-x}K_xBiO_3$. Top: O K spectrum ($x=0.29$). Middle: Ba M_5 spectrum ($x=0.29$). Bottom: Ba $N_{4,5}$ spectrum showing the N_5 (dashed) and N_4 (dotted) components ($x=0$). E_0 equals E_F in the case of the O K and Ba M_5 spectra as well as for the Ba N_4 spectrum. The Ba N_5 component is shifted by the calculated spin-orbit splitting of 2.62 eV [expt. 2.59 eV (Ref. 37)].

sists of two spectra, the N_4 spectrum involving a Ba-$4d_{3/2}$ core hole and the N_5 spectrum involving a Ba $4d_{5/2}$ core hole. The core levels are spin-orbit split by 2.62 eV which is very close to the experimental value of 2.59 eV.[37] Again, the Ba p partial DOS is predominantly mapped. (The atomiclike Ba $5p$ states have been omitted as in the case of PES). It is interesting to note that despite the fact that the N_5 contribution should be larger than the N_4 due to the weighting factors given by the dipole selection rules, the N_4 spectrum outgrows the N_5 spectrum due to the larger matrix elements that actually exist.

As shown in Fig. 10, the relevant Bi site related XES spectra map the Bi d (top panel) and, predominantly, the Bi p (bottom panel) valence-band DOS. The calculation proceeded in analogy to that for the Ba-$N_{4,5}$ spectrum. The Bi N_6 and the Bi N_7 spectra are spin-orbit split by 5.5 eV, which compares well with the experimental value[37] of 5.31 eV as measured by photoemission. Matrix-element differences for the $4f_{7/2}$ core hole (N_7) and the $4f_{5/2}$ (N_6) core hole play an important role in reversing the magnitude of the spectra as compared to the weighting produced by the dipole selection rules.

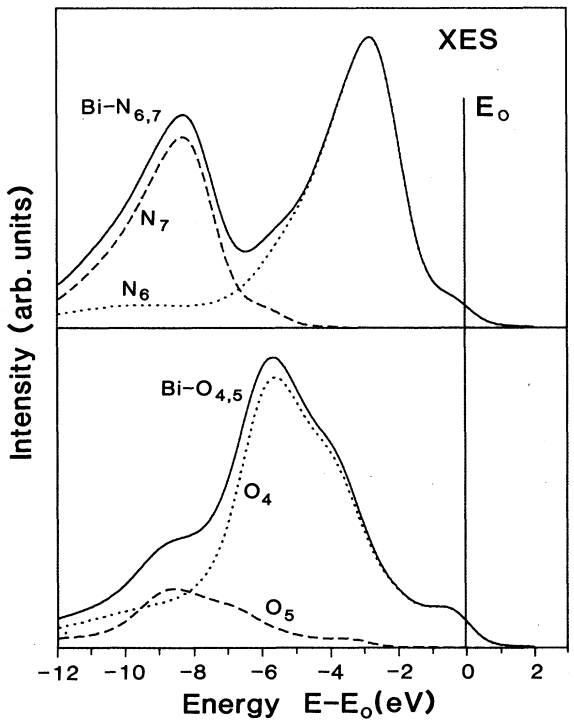

FIG. 10. Calculated x-ray emission spectra for $Ba_{1-x}K_xBiO_3$ ($x=0.29$). Top: Bi $N_{6,7}$ spectrum and the individual N_6 (dotted) and N_7 (dashed contributions). Bottom: Total Bi $O_{4,5}$ spectrum showing the O_5 (dashed) and O_4 (dotted) components. E_0 corresponds to E_F for the Bi N_6 and the Bi O_4 spectrum. The Bi N_7 and Bi O_5 components are shifted by the calculated spin-orbit splittings of 5.5 eV [expt. 5.31 eV (Ref. 37)] and 2.98 eV [expt. 3.05 eV (Ref. 42)], respectively.

This effect is even more important for the Bi-$O_{4,5}$ spectrum, where the O_5 component, i.e., the transition into a Bi-$d_{5/2}$ core hole, is strongly quenched. The spin-orbit splitting between the $5d_{3/2}$ and the $5d_{5/2}$ core level was calculated to be 2.98 eV, again in very good agreement with the experimental value[42] of 3.05 eV.

IV. DISCUSSION OF SUPERCONDUCTIVITY

We will discuss the origin of superconductivity in the Ba-K-Bi-O system together with that of other high-T_c superconductors. There are now some isotope effect measurements for high-T_c superconductors: the α values are 0.2–0.4 for $(BaK)BiO_3$,[6,7] and 0.2–0.6 for $Ba(PbBi)O_3$.[6,43] Although there is some scattering in the measured values, a substantial isotope effect exists for these materials. This clearly shows that phonons are involved in the superconductivity. Therefore, we first try to explain the superconductivity of $(BaK)BiO_3$ by means of the ordinary electron-phonon mechanism, and then we compare the results obtained for the other materials in order to obtain a perspective on the superconducting mechanism for those materials.

We have calculated the McMillan-Hopfield parameters[44] η_j ($\eta_j = N(E_F)\langle I_j^2\rangle$, where $\langle I_j^2\rangle$ is the FS average of the squared matrix element of grad V for atom j) using the rigid muffin-tin approximation (RMTA) of Gaspari and Gyorffy.[45] In order to take into account the effects of Ba-K alloying we use a rigid-band model and fix E_F to the value corresponding to $x=0.29$. This approximation is justified by the fact that the $\langle I_j^2\rangle$ squared matrix element is, to a good extent in our case, independent of the Fermi-level position, so that η_j scales with $N(E_F)$. The values of the η parameters are $\eta_{Ba}=0$, $\eta_{Bi}=0.07$, and $\eta_0=1.71$, in units of eV/Å^2. (These values refer to the unit cell.) The largest contribution by far comes from the oxygen atoms. The O contribution is of the same order as in the case of $La_{2-x}Ba_xCuO_4$ ($x\sim0.15$),[19] while it is much larger than the contribution of the O atoms in the two-dimensional Cu-O plane of $YBa_2Cu_3O_7$,[20] $Bi_2Sr_2CaCu_2O_8$,[21] and $Tl_2Ba_2CaCu_2O_8$ (Ref. 22) (see Table II); note that η_0 was found to be 1 eV/Å^2 for the O atoms in the linear Cu-O chains in $YBa_2Cu_3O_7$.[20] The Bi contribution in $(BaK)BiO_3$ is much smaller than the Cu contribution in the cuprate high-T_c materials. This is because of the smaller relative contribution of Bi to $N(E_F)$. However, the Bi contribution in $(BaK)BiO_3$ is larger than that found[21] for Bi in $Bi_2Sr_2CaCu_2O_8$, $\eta_{Bi}=0.04$ eV/Å^2. This reflects the larger relative contribution of Bi to $N(E_F)$ and, possibly, also the different nature of the Bi-O related states around E_F in the two systems, namely p-p in $Bi_2Sr_2CaCu_2O_8$ (Ref. 21) and s-p in $(BaK)BiO_3$. From a knowledge of η_j and using the Allen and Dynes[46] strong-coupling limit with $\mu^*=0.1$, we can calculate the critical temperature to be $T_c\sim37$ K. A smaller $T_c\sim30$ K (~25 K) is obtained using the McMillan formula and assuming $\Theta_D\sim200$ K (~300 K); a value of $\Theta_D\lesssim200$ is consistent with the measurements of Kitazawa *et al.*[12]

TABLE II. Published values of McMillan-Hopfield parameters η for metal atoms (Ti or Bi or Cu) and O atoms per formula unit as estimated from band-structure calculations. The electron-phonon coupling constants λ and the superconducting transition temperatures T_c are estimated by using Eq. (1) and the McMillan formula for assumed Debye temperatures Θ (=200 and 600 K). Only the contributions of Cu and O are considered for estimating λ and T_c. (The contribution of the one-dimensional chain has been neglected in $YBa_2Cu_3O_7$). Δ is the p-d (or p-s) energy separation estimated from the band-structure calculations. The last column shows the experimental values for T_c.

	η (eV/A^2)		Θ		T_c	Δ	T_c (expt.)
	Cu	O	(K)	λ	(K)	(eV)	(K)
$LiTi_2O_4$	1.96	2.26[a]	200	5.1	36	8[a]	11[f]
	(Ti)		600	0.6	9		
$Ba_{1-x}K_xBiO_3$	0.07	1.71	200	3.0	30	8	27[g]
($x=0.29$)	(Bi)		600	0.3	1		
$La_{2-x}Sr_xCuO_4$	1.11	1.60[b]	200	3.3	31	2[b]	37[h]
($x=0.15$)			600	0.4	1		
$YBa_2Cu_3O_7$	0.32	0.46[c]	200	0.9	11	0[c]	93[i]
			600	0.1	0		
$Bi_2Sr_2CaCu_2O_8$	0.52	0.64[d]	200	1.4	17	0[d]	85[j]
			600	0.2	0		
$Tl_2Ba_2CaCu_2O_8$	0.60	0.88[e]	200	1.8	22	0[e]	110[k]
			600	0.2	0		

[a]Reference 23.
[b]Reference 48.
[c]Reference 20.
[d]Reference 21.
[e]Reference 22.
[f]Reference 13.
[g]Reference 8.
[h]Reference 49.
[i]Reference 4.
[j]Reference 50.
[k]Reference 51.

who found $\Theta_D \leq 190$ K in $BaPb_{1-y}Bi_yO_3$, depending on the y value ($0<y<0.3$).

If we calculate the electron-phonon coupling constant λ as

$$\lambda=\sum_j \frac{\eta_j}{M_j\langle\omega^2\rangle} \tag{1}$$

and assume a Debye model for the phonon spectrum with $\alpha^2(\omega)$ equal to the constant in the spectral function $\alpha^2(\omega)F(\omega)$ (which leads to $\langle\omega^2\rangle=\frac{1}{2}\Theta_D^2$), we obtain $\lambda\sim 3$ (1.4) for $\Theta_D=200$ K (300 K). Thus, for this choice of the parameters involved, this estimation of λ indicates strong coupling in this material. This is in agreement with the conclusions of Kitazawa *et al.*[12] in $BaPb_{1-y}Bi_yO_3$, who obtained a λ value increasing with y, reaching values ~ 1.5 for $y=0.3$ (these authors also assumed a Debye model for the phonon spectrum). Despite the crudeness of the RMTA and the uncertainty in the assumptions made for the phonon spectrum, these calculations indicate that superconductivity in the $(BaK)BiO_3$ system can be understood in terms of the electron-phonon interaction, within a strong-coupling regime. However, doubts about the strong-coupling nature of this system have recently been raised by Batlogg *et al.*;[6] based on the comparison between the bare $N(E_F)$ values and the specific-heat anomaly deduced from the thermodynamic critical field slope (dH_c/dT) for $(BaK)BiO_3$ and $Ba(PbBi)O_3$, they estimated that λ cannot exceed 0.6–0.8. Having these observations in mind, we cannot therefore exclude that, possibly because of the Debye model assumption, our estimate of λ could be wrong. In fact, our RMTA calculations only provide η and, unless the phonon contribution to λ is known, we cannot quantify λ exactly. However, since the weak coupling suggested by Batlogg *et al.*[6] for $(BaK)BiO_3$ contradicts the strong coupling previously indicated for $Ba(BiPb)O_3$ by Kitazawa *et al.*[12] and Batlogg,[47] more experimental work is needed to clarify this point.

In Table II, we summarize the η values for several materials[20–23,48] and give T_c by using the MacMillan formula assuming two values of the Debye temperature together with the experimental values.[4,8,13,49–51] These T_c are estimated by considering only the contributions of Ti and O for $LiTi_2O_4$, of Bi and O for $(BaK)BiO_3$, and of Cu and O in the two-dimensional Cu-O plane for the cuprate materials. The superconductivity of $LiTi_2O_4$ is characterized[23] with a high Debye temperature ($\Theta\sim 600$ K) and weak coupling ($\lambda\sim 0.6$). If the Debye temperature was lower, the material would have higher T_c. However, the crystal has a cubic spinel structure, in which the oxygen atoms have four nearest neighbors (three Ti and one Li) and are tightly bonded to the Ti neighboring atoms. As a result, the Debye temperature is high, which gives the relatively low transition temperature. The other materials are characterized by relatively lower Debye temperatures[52] ($\sim$200–400 K). For $Ba_{0.71}K_{0.29}BiO_3$ ($\Theta\sim 200$ K), the electron-phonon mechanism gives a reasonable explanation for the superconductivity, as mentioned above in detail. For $La_{1.85}Sr_{0.15}CuO_4$, the experimental value of T_c (37 K) is almost the upper limit which can be attained by the electron-phonon mechanism, because these η values give $T_c=41$ K as the strong-coupling limit ($\lambda\rightarrow\infty$): in fact, for realizing $T_c\sim 37$ K, phonons

characterized by $\Theta \sim 100$ K are expected; for example, the soft breathing mode as pointed out by Weber,[53] or the soft tilt mode by Cohen *et al.*[54] For higher-T_c materials, the electron-phonon mechanism is completely insufficient.

We further clarify the differences of the electronic structure between these cuprate and noncuprate materials in relation to the electron-phonon interaction and the charge fluctuations. For $Ba_{1-x}K_xBiO_4$, the η value of O is large, while that of Bi is small; therefore just O vibrations can contribute to T_c, independent of the vibrational spectrum of the other atoms. By contrast, the cuprate materials have the same order of η values for both Cu and O, which means that Cu can contribute to T_c through an appropriate vibrational mode. Another difference is the possibility of dynamical change fluctuations between Cu and O sites which might contribute to raising T_c. Charge fluctuations can be brought about by the virtual transition between the remote bands from the Fermi surface, for example, the transition from Bi 6*s* states around -10 eV to unoccupied O 2*p* states just above the Fermi energy (see Fig. 3). This type of charge fluctuation is characterized by the magnitude of the *p*-*d* separation [the *p*-*s* separation for $(BaK)BiO_3$] Δ which is defined by the difference of the energy levels between O 2*p* and Cu 3*d* (Bi 6*s*) states, as pointed out by Park *et al.*[55] The Δ values which are estimated from the center of gravity of the partial density of states are shown also in Table II. It is seen that the cuprate materials have small Δ values, which implies the importance of charge fluctuations between O 2*p* and Cu 3*d* states. For $LiTi_2O_4$ and $(BaK)BiO_3$, the Δ values are large. The charge fluctuation between Bi and O atoms tends to be suppressed; this factor reinforces the assertion that the electron-phonon mechanism dominates the superconductivity of $(BaK)BiO_3$. We can speculate that the charge-transfer mechanism between Cu and O atoms becomes gradually more important in going from the $(BaK)BiO_3$ system through $(LaSr)_2CuO_4$ to the other cuprate systems. In fact, the isotope effect is sizable ($\alpha = 0.16-0.37$) in $(LaSr)_2CuO$ and is small but finite in the $YBa_2Cu_3O_{7-\delta}$ system. The precise experimental determination of the α value is thus crucial for clarifying the nature of its superconductivity.

ACKNOWLEDGMENTS

We thank Dr. Jaejun Yu for many interesting discussions and for helping us in some aspects of this research. This paper was partially supported by the National Science Foundation (through the Northwestern University Materials Research Center, Grant No. DMR88-21571 and a computing grant from its Division of Advanced Scientific Computing at the National Center for Supercomputing Applications, University of Illinois, Urbana/Champaign, and the Pittsburgh Supercomputing Center) and by the Austrian Fond zur Förderung der Wissenschaftlichen Forschung (Project No. 7064P), by a joint common project of the Austrian Science Foundation and the U.S. National Science Foundation (Grant No. INT84-20207).

*Permanent address: NEC Fundamental Research Laboratories, Miyazaki 4-1-1, Miyamae-ku, Kawasaki 231, Japan.

[1]L. F. Mattheiss, E. M. Gyorgy, and D. W. Johnson, Jr., Phys. Rev. B **37**, 3745 (1988).

[2]R. J. Cava, B. Batlogg, J. J. Krajewski, R. C. Farrow, L. W. Rupp, Jr., A. E. White, K. T. Short, W. F. Peck, Jr., and T. Y. Kometani, Nature **332**, 814 (1988).

[3]J. C. Bednorz and K. A. Müller, Z. Phys. B **64**, 198 (1986).

[4]N. K. Wu, J. R. Ashburn, C. J. Torng, P. H. Hor, R. L. Meng, L. Gao, Z. J. Huang, Y. Q. Wand, and C. W. Chu, Phys. Rev. Lett. **58**, 908 (1987).

[5]For example, see papers in Proceedings of the International Conference on High Temperature Superconductors and Materials and Mechanisms of Superconductivity, Interlaken, Switzerland, 1988 [Physica C **153-155**, 3 (1988)].

[6]B. Batlogg, R. Cava, L. Rupp, A. M. Mujsce, J. J. Krajewski, J. P. Remeika, W. F. Peck, Jr., A. S. Cooper, and G. P. Espinosa, Phys. Rev. Lett. **61**, 1670 (1988).

[7]D. G. Hinks, D. R. Richards, B. Dabrowski, D. T. Marx, and A. W. Mitchell, Nature **335**, 419 (1988).

[8]D. G. Hinks, B. Dabrowski, J. D. Jorgensen, A. W. Mitchell, D. R. Richards, Shiyou Pei, and Donglu Shi, Nature **333**, 836 (1988).

[9]M. T. Weller, J. R. Grasmeder, P. C. Lanchester, P. A. J. de Groot, G. P. Rapson, and A. C. Hannon, Physica C **156**, 265 (1988).

[10]L. F. Schneemeyer, J. K. Thomas, T. Siegrist, B. Batlogg, L. W. Rupp, R. L. Opila, R. J. Cava, and D. W. Murphy, Nature **335**, 421 (1988).

[11]A. W. Sleight, J. L. Gillson, and P. E. Bierstedt, Solid State Commun. **17**, 27 (1975); D. E. Cox and A. W. Sleight, Acta. Crystallogr. B **35**, 1 (1979).

[12]K. Kitazawa, S. Uchida, and S. Tanaka, Physica B **135**, 505 (1985).

[13]M. R. Harrison, P. P. Edwards, and J. B. Goodenough, Philos. Mag. B **52**, 679 (1985), and references therein.

[14]L. F. Mattheiss and D. R. Hamann, Phys. Rev. Lett. **60**, 2681 (1988).

[15]H. J. F. Jansen and A. J. Freeman, Phys. Rev. B **30**, 561 (1984), and references therein.

[16]L. F. Mattheiss and D. R. Hamann, Phys. Rev. B **28**, 4227 (1983).

[17]J. Yu, A. J. Freeman, and J.-H. Xu, Phys. Rev. Lett. **58**, 1035 (1987); A. J. Freeman, J. Yu, and C. L. Fu, Phys. Rev. B **36**, 7111 (1987).

[18]L. F. Mattheiss, Phys. Rev. Lett. **58**, 1028 (1987).

[19]W. E. Pickett, H. Krakauer, D. A. Papaconstantopoulos, and L. L. Boyer, Phys. Rev. B **35**, 7252 (1987).

[20]S. Massidda, J. Yu, A. J. Freeman, and D. D. Koelling, Phys. Lett. A **122**, 198 (1987); J. Yu, S. Massidda, A. J. Freeman, and D. D. Koelling, *ibid.* **122**, 203 (1987).

[21]S. Massidda, J. Yu, and A. J. Freeman, Physica C **152**, 251 (1988).

[22]J. Yu, S. Massidda, and A. J. Freeman, Physica C **152**, 273 (1988).

[23]S. Massidda, J. Yu, and A. J. Freeman, Phys. Rev. B **38**,

11 352 (1988).
[24]J. Redinger, P. Marksteiner, and P. Weinberger, Z. Phys. B **63**, 321 (1986).
[25]H. Winter, P. J. Durham, and G. M. Stocks, J. Phys. F **14**, 1047 (1984).
[26]U. von Barth and G. Grossman, Solid State Commun. **32**, 645 (1979).
[27]U. von Barth and G. Grossman, Phys. Rev. B **25**, 5150 (1982).
[28]J. Redinger, J. Yu, A. J. Freeman, and P. Weinberger, Phys. Lett. A **124**, 463 (1987).
[29]J. Redinger, A. J. Freeman, J. Yu, and S. Massidda, Phys. Lett. A **124**, 469 (1987).
[30]P. Marksteiner, S. Massidda, J. Yu, A. J. Freeman, and J. Redinger, Phys. Rev. B **38**, 5098 (1988).
[31]P. Marksteiner, S. Massidda, J. Yu, A. J. Freeman, J. Redinger, and P. Weinberger, Phys. Rev. B **39**, 2894 (1989).
[32]E. Beauprez, C. F. Hague, J.-M. Mariot, F. Teyssandier, J. Redinger, P. Marksteiner, and P. Weinberger, Phys. Rev. B **34**, 886 (1986).
[33]R. S. List, A. J. Arko, Z. Fisk, S.-W. Cheong, S. D. Conradson, J. D. Thompson, C. B. Pierce, D. E. Peterson, R. J. Bartlett, N. D. Shinn, J. E. Schirber, B. W. Veal, A. P. Paulikas, and J. C. Campuzano, Phys. Rev. B **38**, 11 966 (1988); A. J. Arko, R. S. List, Z. Fisk, S.-W. Cheong, J. D. Thompson, J. A. O'Rourke, C. G. Olson, A.-B. Yang, Tun-Wen Pi, J. E. Schirber, and N. D. Shinn, J. Magn. Magn. Mater. **75**, L1 (1988).
[34]A. J. Arko, Bull. Am. Phys. Soc. **34**, 809 (1989); A. J. Arko *et al.*, *ibid.* **34**, 690 (1989); R. S. List *et al.*, *ibid.* **34**, 691 (1989); J. C. Campuzano *et al.*, *ibid.* **34**, 840 (1989).
[35]J. Ghijsen, L. H. Tjeng, J. van Elp, H. Eskes, J. Westerink, G. A. Sawatzky, and M. T. Czyzyk, Phys. Rev. B **38**, 11 322 (1988).
[36]A. Fujimori and F. Minami, Phys. Rev. B **30**, 957 (1984).
[37]G. K. Wertheim, J. P. Remeika, and D. N. E. Buchanan, Phys. Rev. B **26**, 2120 (1982).
[38]K. Takegahara and T. Kasuya, J. Phys. Soc. Jpn. **56**, 1487 (1987).
[39]A. Fujimori, K. Kawakami, and N. Tsuda, Phys. Rev. B **38**, 7889 (1988).
[40]H. Sakamoto, H. Namatame, T. Mori, K. Kitazawa, S. Tanaka, and S. Suga, J. Phys. Soc. Jpn. **56**, 365 (1987).
[41]E. J. McGuire, Phys. Rev. A **2**, 273 (1970); **3**, 587 (1971).
[42]S. Tajima, H. Ishii, I. Rittaporn, S. Uchida, S. Tanaka, K. Kitazawa, M. Seki, and S. Suga, Phys. Rev. B **38**, 1143 (1988).
[43]H. C. zur Loye, K. J. Leary, S. W. Keller, W. K. Ham, T. A. Faltens, J. N. Michaels, and A. M. Stacy, Science **238**, 1558 (1987).
[44]W. L. McMillan, Phys. Rev. **167**, 331 (1968); J. J. Hopfield, *ibid.* **186**, 443 (1969).
[45]G. D. Gaspari and B. L. Gyorffy, Phys. Rev. Lett. **28**, 801 (1972).
[46]P. B. Allen and R. C. Dynes, Phys. Rev. B **12**, 905 (1975).
[47]B. Batlogg, Physica **B126**, 275 (1984).
[48]Private communication from J. Yu based on the calculation in Ref. 17.
[49]R. B. van Dover, R. J. Cava, B. Batlogg, and E. A. Rietman, Phys. Rev. B **35**, 5337 (1987).
[50]J. M. Tarascon, W. R. McKinnon, P. Barboux, D. M. Hwang, B. G. Bagley, L. H. Greene, G. W. Hull, Y. LePage, N. Stoffel, and M. Giround, Phys. Rev. B **38**, 8885 (1988).
[51]M. A. Subramanian, J. C. Calabrese, C. C. Torardi, J. Gopalakrishnan, T. R. Askew, R. B. Flippen, K. J. Morrissey, U. Chowdhry, and A. W. Sleight, Nature **332**, 420 (1988).
[52]D. Eckert, A. Janod, A. Bezinge, T. Graf, and J. Müller, J. Low Temp. Phys. **73**, 241 (1988).
[53]W. Weber, Phys. Rev. Lett. **58**, 1371 (1987).
[54]R. E. Cohen, W. E. Pickett, and H. Krakauer, Phys. Rev. Lett. **62**, 831 (1989); P. Böni, J. D. Axe, G. Shirane, P. J. Picone, and T. R. Thurston, Phys. Rev. B **38**, 185 (1988).
[55]K. T. Park, K. Terakura, T. Oguchi, A. Yanase, and M. Ikeda, J. Phys. Soc. Jpn. **57**, 3445 (1988).